Simulation of an Internal Nozzle Flow Using an Euler-Lagrange Method

[1]Andreas Peters*; [1]Udo Lantermann; [1]Ould el Moctar

[1]*University of Duisburg-Essen, Duisburg, Germany*

Abstract

In this work, an Euler-Lagrange method to simulate cavitation and predict cavitation erosion is presented. The method considers bubble motions as well as growth and collapse of a discrete number of single, spherical bubbles. A two-way coupling approach is implemented so that both liquid phase and vapour bubbles interact with each other. In contrast to Euler-Euler methods, this allows a more detailed simulation of bubble transport and dynamics. We used the developed method to simulate the internal cavitating flow in a nozzle.

Keywords: Euler-Lagrange, cavitation, erosion, particle tracking, bubble dynamics

Introduction

Hydrodynamic cavitation is a process of evaporation caused by liquid pressures below the equilibrium vapour pressure at constant temperature. Depending on water quality, flows of liquid water contain a certain amount of free gas bubbles. When these bubbles reach regions of low pressure in a flow they grow due to evaporation processes which start on the bubble walls. This growth continues until they reach regions of higher pressure again. The condensation processes start on the bubble walls causing the bubbles to rapidly collapse. As these collapses take place, high pressures are generated in the bubbles' centres and pressure waves are radiated through the fluid. These pressure waves are attenuated as they travel further through the fluid so that the pressure amplitudes become smaller. Though, if a bubble is located in the vicinity of a solid surface, the bubble pressure after the collapse or the formation of a liquid water jet, the so-called *microjet*, may lead to material damage. First, this erosion process causes plastic deformation of the material during the so-called *incubation time*. Second, after a longer exposure time, the material will break and mass loss will occur.

The Euler-Lagrange approach considers a continuous liquid phase and a discrete number of spherical vapour bubbles. In contrast to an Euler-Euler method where both phases are continuous and share equal streamlines, the motions of the single bubbles can differ from the streamlines of the liquid phase depending on multiple forces acting on the bubbles. The dynamics of each single bubble are calculated based on the forces acting on the bubble wall using the Rayleigh-Plesset equation. This equation can be solved iteratively to obtain the bubble wall velocity and acceleration and therefore calculate a new bubble radius. The phases are two-way coupled. Thus, both phases influence each other.

In technical applications, flows of high flow gradients are common. Here, the bubbles' traces may differ significantly from the streamlines of the liquid flow. These deviations are large for vortical flows, flows around sharp edges near the tips of propeller blades or flows in rudder gaps. In addition, a better understanding of bubble collapses near surfaces and erosion mechanisms can be gained from analysing the behaviour of single bubbles. Euler-Lagrange methods were used to investigate details of cavitation in flows around propellers, hydrofoils and other technical applications [1-3]. Especially for vortical flows [1] and cloud collapses [4] the Euler-Lagrange method was used to provide more detailed insights into the regarded physical processes. In this work, we used the Euler-Lagrange method to simulate the internal cavitating flow in an axisymmetric nozzle and to predict cavitation erosion from the information about flow properties.

Numerical Method

We used the open source CFD framework OpenFOAM to combine Lagrangian particles with a Reynolds-averaged Navier-Stokes solver. For the multiphase flow on an Eulerian grid, we solved the equations of mass and momentum conservation. During one Eulerian time step, multiple time steps of the Lagrangian transport of the single bubbles may be calculated depending on bubble velocity and growth related to the grid size. The Lagrangian equation of motion reads as [1]

*Corresponding Author, Andreas Peters: andreas.peters@uni-due.de

$$m\frac{d\boldsymbol{u}_b}{dt} = \sum_i \boldsymbol{F}_i \,.$$

$m = m_b + m_a$ is the effective bubble mass. $m_b = \rho_b V_b$ is the bubble mass with the bubble density ρ_b and bubble volume V_b. $m_a = \frac{1}{2}\rho_l V_b$ is the added mass with ρ_l as the liquid density. $\boldsymbol{u}_b$ is the bubble velocity and t is the time. $\boldsymbol{F}_i$ are forces acting on a bubble due to pressure gradient, virtual mass, drag, volume variation, lift and gravity. The bubble position $\boldsymbol{x}_b$ can then be obtained by integrating its velocity over time:

$$\frac{d\boldsymbol{x}_b}{dt} = \boldsymbol{u}_b \,.$$

After the Lagrangian equation is solved and the new bubble position is defined the bubble dynamics are calculated. The dynamics of a cavitation bubble take place in even shorter time scales than the bubble motions and are, therefore, integrated in an internal time loop. The time steps are adjustable and become smallest during the collapse phase of a bubble. The equation of bubble dynamics is based on the Rayleigh-Plesset equation. Following the work of Brennen [5] and Chahine [3] it reads as

$$\frac{p_b - p}{p} - \frac{2\sigma}{\rho_l R} - \frac{4\nu}{R}\dot{R} + \frac{(\boldsymbol{u} - \boldsymbol{u_b})^2}{4} = R\ddot{R} + \frac{3}{2}\dot{R}^2 \,.$$

$p_b = p_v + p_g$ is the pressure inside of the bubble where p_v is the vapour pressure and p_g the pressure of non-condensable gas. p is the pressure in the liquid carrier phase at the position of the bubble. σ and ν are the surface tension and kinematic viscosity of liquid water, respectively. $\boldsymbol{u}$ is the velocity of the carrier phase flow. $R, \dot{R}\ and\ \ddot{R}$ are the bubble radius, bubble wall velocity and bubble wall acceleration. Using this equation we can determine if a bubble is going to grow or shrink.

Dynamics and transport of the bubbles are influenced by forces coming from the carrier phase. The bubbles will influence the carrier phase because of their own motion which is transferred to the momentum equation and because they change mixture density $\rho = \alpha_v\rho_v + (1-\alpha_v)\rho_l$ and viscosity $\mu = \alpha_v\mu_v + (1-\alpha_v)\mu_l$, where the indices l and v stand for liquid and vapour phase, respectively. The vapour volume fraction $\alpha_v = V_v/V$ is the volume of vapour V_v in a regarded cell of volume V. The volume of vapour in a control volume is obtained based on the volume of accumulated bubbles in the control volume. Furthermore, the Poisson equation which is used to calculate the pressure in the flow contains source terms depending on the vapour volume fraction. We chose the approach by Sauer and Schnerr [6] to calculate these source terms.

To predict erosion, we used the erosion model by Peters et al. [9], based on the microjet hypothesis by Dular and Coutier-Delgosha [11]. We hypothesise that a bubble will collapse asymmetrically if it is positioned close to a surface. This asymmetric collapse causes the formation of a high velocity microjet, which is almost always directed towards the surface. Depending on the liquid pressure at the bubble wall, the bubble is collapsing more or less rapidly and creates a microjet which may damage the surface. The dimensionless coefficient c_{Def} was introduced [9] to predict erosion sensitive areas taking into account the amount of impacts and the impacts' intensities in an area. The erosion model uses information from the flow solution including the vapour volume fraction which, in this work, was calculated based on the bubble distribution in the domain.

Results

The cavitating flow through an axisymmetric nozzle has been investigated experimentally [7-8] and numerically [9-10] before. A sketch of the nozzle cross section is shown in Figure 1. Water flowed from top to bottom through an inlet cylinder and radially outwards through a radial divergent part. The two parts were connected by an 1 mm radius at which unsteady cavitation was generated. In the experiments, the bottom surface of the radial divergent part functioned as a probe on which erosion occurred in a defined radial distance from the rotation axis of the geometry. We generated a numerical simulation domain from 0° to 22.5° of the full 360° geometry. The domain was discretised with a cylindrical mesh using hexahedral control volumes.

*Corresponding Author, Andreas Peters: andreas.peters@uni-due.de

Figure 2 shows the shedding and collapse processes of different bubble clouds (grey) from the side. The pressure is depicted on a plane behind the cloud with low pressures shown in blue and high pressures shown in red. Two clouds were shed from the radius and travelled further downstream. The upper cloud touches the top of the domain. We can see that bubbles follow this cloud from the cavitation region at the connecting radius. The lower cloud has been separated from other cavitation regions and touches the bottom surface while encountering a region of higher pressure again. The lower cloud was collapsing shortly after the depicted moment when it encountered higher liquid pressures further downstream. The collapse of this cloud generated high pressures traveling through the domain and causing the upper cloud to collapse as well. While both clouds started to collapse, another cloud was generated at the connecting radius.

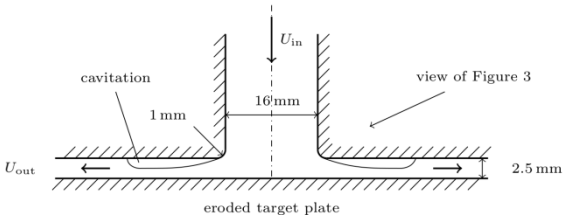

Figure 1: sketch of nozzle cross section taken from [9]

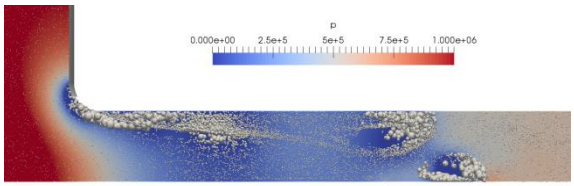

Figure 2: side view of cavitation bubbles collapsing near the bottom surface

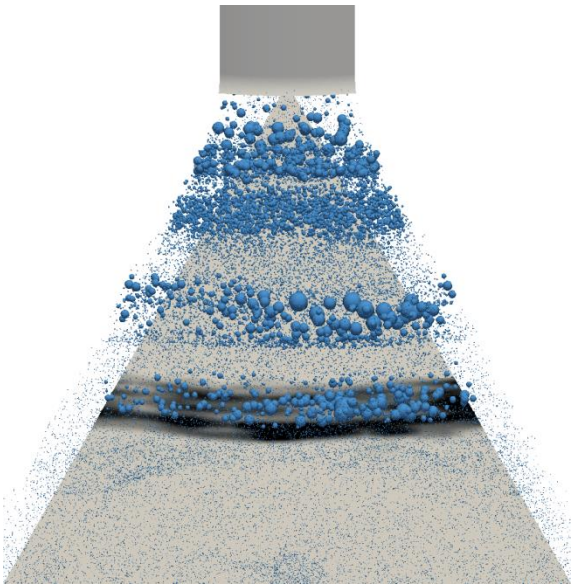

Figure 3: perspective view of cavitation bubbles and erosion prediction into axisymmetric nozzle

Figure 2 shows the shedding and collapse processes of different bubble clouds (grey) from a side view into the nozzle. The pressure is depicted on a plane behind the cloud with low pressures shown in blue and high pressures shown in red. Two clouds were shed from the radius and travelled further downstream. The upper cloud touches the top of the domain. We can see that bubbles follow this cloud from the cavitation region at the connecting radius. The lower cloud has been separated from other cavitation regions and touches the bottom surface while encountering a region of higher pressure again. The lower cloud was collapsing shortly after the depicted moment when it encountered higher liquid pressures further downstream. The collapse of this cloud generated high pressures traveling through the domain and causing the upper cloud to collapse as well. While both clouds started to collapse, another cloud was generated at the connecting radius.

Figure 3 shows a perspective view into the nozzle as denoted in the sketch of Figure 1. The same time instant is shown as in Figure 2. The outer wall of the inlet cylinder and the connecting radius are shown in grey. The bottom of the radial outlet part is shown in grey as well whereas the top is made transparent. The growth of the cavitation bubbles (blue) starts at the radius. They are accumulated and form bubble clouds which travel further downstream and collapse in regions of higher liquid pressure. The black area on the bottom surface shows the erosion prediction by the microjet erosion model. Most clouds collapse in the vicinity of the area predicted to be eroded.

The cloud collapse and cloud shedding processes reoccurred periodically and with different intensities. The vapour volume in the simulation domain changed as new clouds were generated and cavitation regions collapsed. Furthermore, high forces were exerted on the bottom surface of the nozzle when cavitation clouds collapsed near the surface.

*Corresponding Author, Andreas Peters: andreas.peters@uni-due.de

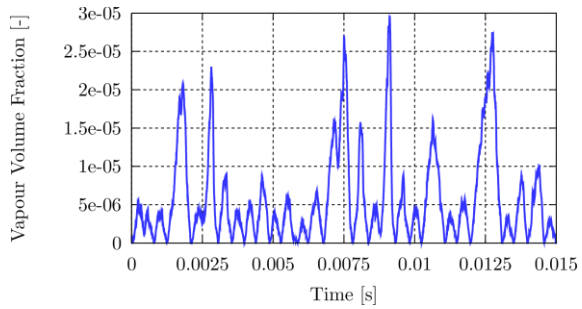

Figure 1: weight averaged vapour volume fraction

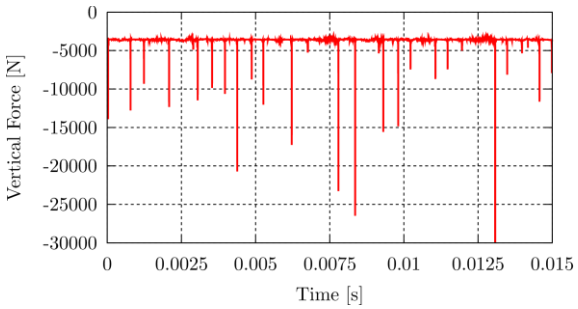

Figure 2: vertical force on the bottom surface

Figure 4 shows the temporal progress of the vapour volume fraction in the simulation. The volume fraction was weight averaged taking the cell volumes into account. The vapour volume oscillated periodically with different frequencies. Oscillations of higher frequencies were of lower amplitudes whereas oscillations of lower frequencies were of higher amplitudes. Figure 5 shows the time history of the vertical force on the bottom boundary. The average magnitude of the vertical force was about 3600 N. Peaks of large negative forces appeared harmonically. The peaks exceeded this value by a factor of 2 to 10. Analysing the frequencies of the time history of the force with a fast Fourier transform, we obtained a characteristic frequency of about 2000 Hz. This frequency corresponded to the negative peaks in the vertical force as well as to the high frequency oscillations in vapour volume. We concluded that these high magnitude force peaks were caused by collapsing clouds of cavitation bubbles. A fast Fourier transform of the time history of the volume fraction did not yield a clear characteristic frequency, probably because of the fact that the simulation should have been run for a longer time.

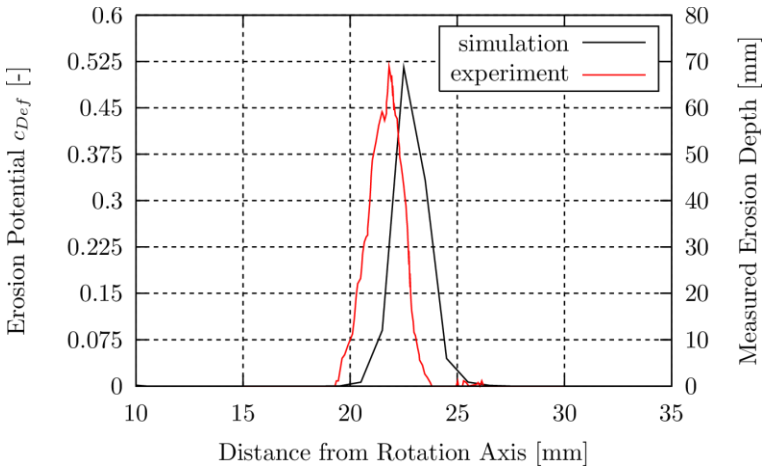

Figure 3: numerical erosion prediction (red) and experimentally measured erosion depth (black) [7] on the bottom surface

Figure 6 shows radial distribution of the numerical prediction and the experimental measurement of erosion [7] on the bottom surface of the nozzle. In the experiments, eroded areas were summed up over the circumference of the nozzle for different radial intervals. This approach was also used for the distribution of the numerical coefficient of erosion potential c_{Def} using intervals of 1 mm. The maximum of measured erosion depth was found to be at a distance of 21.8 mm from the central. The maximum erosion potential was calculated close to the measured maximum within an interval of 22 mm to 23 mm. The overall shape of the predicted erosion distribution agreed well with the experiment. Deviations in the maximum of the distributions may be accounted for by the nuclei distribution in the numerical simulation because it has a large influence on the inception and extent of cavitation.

Conclusions and Outlook

We have shown the ability of the Euler-Lagrange approach to simulate hydrodynamic cavitation and enable the prediction of cavitation induced erosion. The consideration of single bubbles ensures a more accurate simulation of

*Corresponding Author, Andreas Peters: andreas.peters@uni-due.de

the bubbles' behaviour. First simulations have shown that cavitation behaviour as well as erosion prediction will differ with variation of the nuclei distribution in the domain which will be investigated in further work. In the future, the present approach enables the possibility to quantitatively predict erosion by correlating bubble collapse rates with pitting patterns from experimental tests.

Acknowledgement

The present work was funded by the German Research Foundation [grant number EL 611/2-1].

References

[1] Abdel-Maksoud, M., Hänel, D., Lantermann, U. (2010). *Modeling and computation of cavitation in vertical flow*. International Journal of Heat and Fluid Flow. 31(6).

[2] Yakubov, S., Cankurt, B., Maquil, T., Schiller, P., Abdel-Maksoud, M., Rung, T. (2011). *Euler-Euler and Euler-Lagrange Approaches to Cavitation Modelling in Marine Applications*. International Conference on Computational Methods in Marine Engineering (MARINE), Lisbon, Portugal.

[3] Chahine, G. L. (2008). *Numerical Simulation of Bubble Flow Interactions*. Cavitation: Turbo-machinery & Medical Applications, WIMRC Forum, Warwick, United Kingdom.

[4] Ma, J., Hsiao, C.-T., Chahine, G. L. (2015). *Euler-Lagrange Simulations of Bubble Cloud Dynamics Near a Wall*. Journal of Fluids Engineering. 137.

[5] Brennen. C. E. (2005). *Fundamentals of Multiphase Flows*. Cambridge University Press. ISBN 0521 848040.

[6] Sauer, J., Schnerr, G. H. (2000). *Unsteady Cavitating Flow – a New Cavitation Model Based on Modified Front Capturing Method an Bubble Dynamics*. In Proceedings of FEDSM, 4th Fluids Engineering Summer Conference.

[7] Franc, J.-P., Riondet, M. (2006). *Incubation Time and Cavitation Erosion Rate of Work-Hardening Materials*. In Proceedings of the 6th International Symposium on Cavitation, CAV2006, Wageningen, Netherlands.

[8] Franc, J.-P., Riondet, M., Karimi, A., Chahine, G. (2011). *Impact Load Measurements in an Erosive Cavitating Flow*. Journal of Fluids Engineering. 133(12).

[9] Peters, A., Sagar, H., Lantermann, U., el Moctar, O. (2015). *Numerical Modelling and Prediction of Cavitation Erosion*. Wear. 338-339.

[10] Peters, A., Lantermann, U., el Moctar, O. (2015). *Numerical Modelling and Prediction of Erosion Induced by Hydrodynamic Cavitation*. Journal of Physics: Conference Series. 656(012054).

[11] Dular, M., Coutier-Delgosha, O. (2009). *Numerical modelling of cavitation erosion*. International Journal for Numerical Methods in Fluids. 61.

*Corresponding Author, Andreas Peters: andreas.peters@uni-due.de